Article

Boosted Electrochemical Immunosensing GM Crops Markers Using Nanobody and Mesoporous Carbon

Mingming Zhang, Guanghui Li, Qing Zhou, Deng Pan, Min Zhu, Runyu Xiao, Yuanjian Zhang, Guoqiu Wu, Yakun Wan, and Yanfei Shen

ACS Sens., **Just Accepted Manuscript** • DOI: 10.1021/acssensors.8b00011 • Publication Date (Web): 19 Feb 2018

Boosted Electrochemical Immunosensing GM Crops Markers Using Nanobody and Mesoporous Carbon

Mingming Zhang[1,3], Guanghui Li[2], Qing Zhou[1], Deng Pan[1], Min Zhu[2], Runyu Xiao[1], Yuanjian Zhang[1], Guoqiu Wu*[1,3], Yakun Wan*[2] and Yanfei Shen*[1]

[1] Medical School, School of Chemistry and Chemical Engineering, Southeast University, Nanjing, Jiangsu 210009, China

[2] Shanghai Novamab Biopharmaceuticals Co., Ltd., Shanghai 201203, China

[3] Center of Clinical Laboratory Medicine of Zhongda Hospital, Southeast University, Nanjing, 210009, China

Email: Yanfei.Shen@seu.edu.cn (Y. Shen); ykwan@novamab.com (Y. Wan); nationball@163.com (G. Wu).

Abstract

The problems of environmental security and the potential risks of human health caused by transgenic crops have aroused numerous attention. Recent studies reveal 5-enolpyruvylshikimate-3-phosphate synthase (EPSPS) from *Agrobacterium* sp. strain CP4 protein (CP4-EPSPS), which shows very high resistance to herbicide glyphosate, is a typical biomarker of genetically modified (GM) crops. For this reason, it is highly anticipated to devise a sensitive and convenient strategy to detect CP4-EPSPS protein in crops. Herein, we reported a simple electrochemical immunosensor by coupling nanobody, ordered mesoporous carbon (OMC), and thionine (Th). As a capture agent, the nanobody was screened out from an immunized Bactrian camel, and exhibited superior properties with respect to conventional antibody, such as higher stability and stronger heat resistance. Moreover, OMC offered an effective platform with high surface area, electrical conductivity and biocompatibility, which greatly facilitated the assembling of redox probe Th, and further coupling of large amount of capture nanobodies. As a result, the CP4-EPSPS protein could be determined with high sensitivity and efficiency by differential pulse voltammetry (DPV) in a wide linear range from 0.001 to 100 ng•mL^{-1} with a low detection limit of 0.72 pg•mL^{-1}, which was more than 3 orders of magnitude lower than those of previously reported works. As an example, the proposed electrochemical immunosensor was successfully applied to spiked samples, demonstrating its great potentials in CP4-EPSPS screening and detection.

Keywords

electrochemical immunoassay, mesoporous carbon, nanobody, genetically modified (GM) crops, CP4-EPSPS

With the development of gene engineering, the use of genetically modified (GM) crops becomes more and more widespread.[1,2] Although transgenic technology can contribute to the increase of crop productivity and quality and depress the use of pesticides, the environmental security problems and potential risks on human health brought by transgenic crops are still controversial.[3-5] Since most of these GM crops contain a gene called 5-enolpyruvylshikimate-3-phosphate synthase (EPSPS) from *Agrobacterium* sp. strain CP4 (CP4-EPSPS), which shows very high resistance to herbicide glyphosate (N-phosphonomethylglycine), the CP4-EPSPS can be regard as a potential biomarker for GM crops screening.[6,7] Thus, it is important to develop a highly sensitive and specific strategy for the detection of CP4-EPSPS in agroproducts. Recently, a few strategies have been developed for the determination of CP4-EPSPS such as polymerase chain reaction (PCR),[8-10] loop-mediated isothermal amplification,[11] liquid chromatography tandem mass spectrometry (LC-MS/MS),[12] surface plasmon resonance (SPR),[13] ELISA and Western bolt.[14,15] However, these detections either are less sensitive and time-consuming, or require expensive equipment or skilled operators. Therefore, it is still of great challenge to develop a more facile and reliable strategy for CP4-EPSPS detection.

Among various alternatives, electrochemical immunosensor[13] possesses numerous advantages such as low detection limits, high sensitivity and specificity, cost efficiency, ease of operation and compact instrumentation that is compatible with portable devices, which have attracted burgeoning attention.[16-21] Moreover, of note, ordered mesoporous carbon (OMC), a vital member of the carbon-based material family, has been widely used in the biosensor due to its excellent thermal/mechanical stability, good electrical conductivity, and biocompatibility.[22-26] The porous feature of OMC allows loading of large number of functional molecules and provides a protective microenvironment for biomolecules to retain their stability and activity. In addition, the straight and short mesochannels and the excellent electric conductivity provide a highway for the electron transportation.[27] Thus, in cooperation with Au nanoparticles for a reliable bioconjugation, OMC could be an attractive support for

biomolecules and probe molecules. On the other hand, nanobody (Nb), or sometimes named as variable domain of the heavy chain (VHH), is the smallest antigen binding fragment and naturally existing in the serum of camels.[28] Compared with conventional antibody, Nb has unique physical and chemical properties such as small molecular size (~15 KDa), high thermal stability and solubility.[29-31] Therefore, by combination the merits of OMC and Nb along with electrochemical method may provide a highly facile and reliable way to detect CP4-EPSPS protein.

Herein, we report an electrochemical immunosensor, where OMC was employed as an effective sensing platform, Nb as capture antibody and Th as an electrochemical probe, to detect CP4-EPSPS protein with high sensitivity and selectivity (Scheme 1). The use of Nb-assisted electrochemical immunoassay based on OMC should have broad application in the fields of food safety and clinical diagnosis.

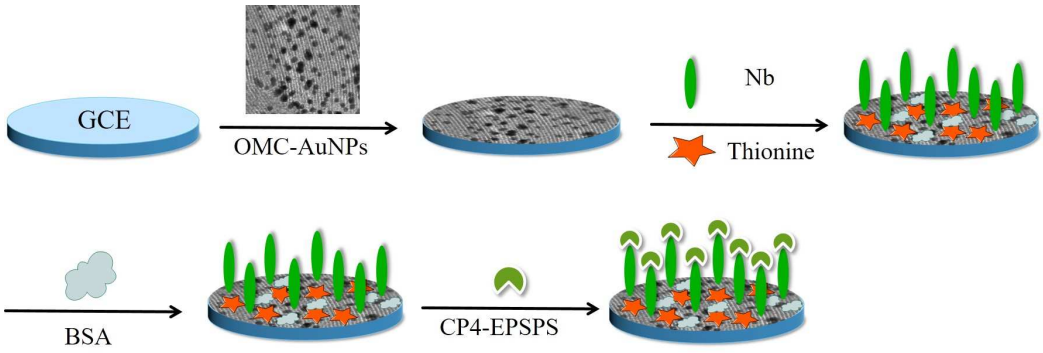

Scheme 1. General process for the Nb-based immunosensor fabrication.

Experimental Section

Materials and Reagents

CP4-EPSPS and other toxins were purchased from YouLong Bio. Co., Ltd. The anti CP4-EPSPS Nb was obtained by immunizing a healthy Bactrian camel with CP4-EPSPS-His antigen according to our previous report.[32] Bovine serum albumin (BSA), Thionin acetate salt (Th), 1-ethyl-3-(3-(dimethylamino) propyl) carbodiimide (EDC), N-hydroxysuccinimide (NHS) and chloroauric acid ($HAuCl_4$) were purchased from Sigma-Aldrich (Shanghai, China). Mesoporous carbon (CMK-3) was obtained

from XFNANO Materials Tech Co. (Nanjing, China). Potassium hexacyanoferrate (□) ($K_3[Fe(CN)_6]$), trisodium citrate ($Na_3C_6H_5O_7$) and potassium chloride (KCl) were purchased from LingFeng Chemical Reagent Co., Ltd (Shanghai, China). Phosphate buffer solution (PBS, 0.1 M, pH 7.4) used in this work was prepared using 0.1 M Na_2HPO_4•$12H_2O$, 0.1 M NaH_2PO_4•$2H_2O$ and 0.1 M KCl. Ultrapure water was obtained from Millipore water purification system (18.2 MΩ•cm).

Apparatus

Cyclic voltammetry (CV) and differential pulse voltammetry (DPV) were performed using a CHI 660E workstation (CHI, USA) at room temperature. All experiments were carried out using a conventional three-electrode system. The modified electrode was used as the working electrode, the counter electrode was a platinum wire and the reference electrode was a Ag/AgCl (3 M KCl). The DPV measurements were performed in N_2-saturated PBS (0.1M, pH 7.4) with 50 ms pulse width, 50 mV pulse amplitude, 0.5 s pulse period and a voltage range from 0 to -0.45 V. Transmission electron microscope (TEM) images and high resolution transmission electron microscope (HRTEM) images were obtained from a JEOL 2100 transmission electron microscope. Scanning electron microscopy (SEM) images were obtained from a ZEISS Ultra Plus scanning electron microscope. Brunauer–Emmett–Teller (BET) surface area was calculated from 77 K N_2 adsorption-desorption isotherms by NovaWin 1000e (Quantachrome, USA). UV-visible absorption spectra (UV-vis) were recorded on a Cary100 UV-vis spectrophotometer (Agilent, USA).

Preparation of AuNPs and OMC-AuNPs

Gold nanoparticles (AuNPs) were synthesized according to previous report.[33] Briefly, 100 mL of 0.01% (w/v) chloroauric acid ($HAuCl_4$) solution was heated to 95°C under reflux, and then, 2.5 mL of 38.8 mM trisodium citrate ($Na_3C_6H_5O_7$) was added to the $HAuCl_4$ solution while stirring. The mixture was heated for another 15 min. After that, the solution was left to room temperature. The as-prepared AuNPs were mixed with 30 mg OMC and the mixture was then stirred for 4 h to form stable OMC-AuNPs composite.[34,35] Finally, the OMC-AuNPs composite was collected by using a 0.22-μm

nylon membrane filter and dried in a vacuum for 1 h. The as-prepared OMC-AuNPs was dispersed in N, N-dimethylformamide (DMF) to form a homogeneous suspension with ultrasonic treatment for further use. The Th/OMC-AuNPs sample for UV-vis measurement was prepared as follows. Briefly, 500 μL of as-prepared OMC-AuNPs suspension (0.1 mg•mL^{-1}) was mixed with 50 μL of the mixture solution of EDC (20 mg•mL^{-1}) and NHS (10 mg•mL^{-1}), and sonicated at room temperature for 2 h. Then 500 μL of Th (0.1 mg•mL^{-1}) was added and the solution was sonicated for another 1 h. After that, the above solution was centrifugated and the precipitation was redispersed in 500 μL DMF for further UV-vis measurement. The concentration of Th and OMC-AuNPs solution for the UV-vis measurement was 0.1 mg•mL^{-1}.

Electrochemical Immunosensor Fabrication

Prior to immunosensor fabrication, a bare glassy carbon electrode (GCE, d=3 mm) was polished with 0.3 and 0.05 μm alumina slurries respectively, and washed by ultrasonic cleaning in ethanol and ultrapure water. Then, GCE surface was coated with 5 μL of the OMC-AuNPs nanocomposite suspension (0.5 mg•mL^{-1}) and dried at room temperature for 24 h. Next, the GCE was rinsed with water and 10 μL of the mixture solution of EDC (20 mg•mL^{-1}) and NHS (10 mg•mL^{-1}) was added onto GCE for 2 h as covalent binding agents to link the amino group on Nb with the carboxyl group on AuNPs. Following rinsing with water, 10 μL of the mixture of Th (100 μg•mL^{-1}) and Nb (10 μg•mL^{-1}) in 0.1 M PBS was incubated on the surface of the electrode at 4°C for 12 h. After rinsing, 10 μL 1% (w/v) of BSA solution was dropped onto the GCE at room temperature for 30 min to block the non-specific binding sites. The modified electrode was incubated with different concentrations of CP4-EPSPS samples for 2 h at room temperature after washing. Finally, the resulting immunosensor was washed with water and stored at 4°C for further use.

Preparation of Spiked Soybean Samples

The spiked samples were prepared by spiking CP4-EPSPS protein into nontransgenic soybean samples. Briefly, 10 mL of the protein extraction solution (0.1 M PBS containing 0.1% BSA and 0.05% Tween-20) was added into 1 g of the dried and

homogenized soybean powder samples. After a gentle shaking at room temperature for 2 h, the suspensions were centrifuged at 10000 g for 10 min. Then, the supernatant was diluted 1000 folds by 0.1 M PBS and spiked with CP4-EPSPS with three different concentrations (1, 10, and 100 ng•mL^{-1}). The mixed extracts were used for sample analysis by the constructed electrochemical immunoassay, and each spiked sample was analyzed with three sets of parallel control. The final concentration of spiked samples was determined by the interpolation method according to the standard calibration plot.

Results and Discussion

Synthesis and Characterization of OMC-AuNPs Nanocomposites

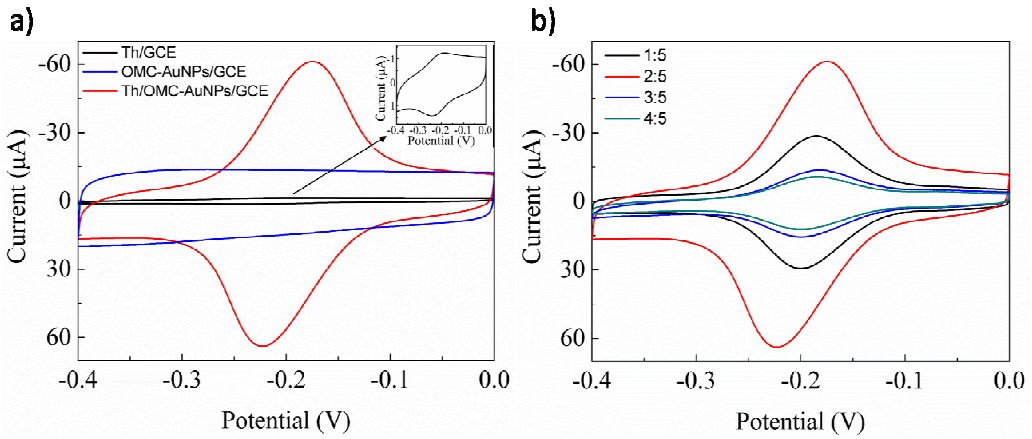

Figure 1. a) CV curves of Th/GCE, OMC-AuNPs/GCE and Th/OMC-AuNPs/GCE (AuNPs/OMC=2:5), and b) CV curves of Th/OMC-AuNPs/GCE with different ratios of AuNPs to OMC in N_2-saturated PBS (0.1 M, pH 7.4). Scan rate: 100 mV•s^{-1}. The inset in a) is the enlarged CV curve of Th/GCE.

For a reliable conjugation of OMC and Nb, AuNPs were immobilized on OMC as a friendly connection between them. Briefly, OMC-AuNPs was prepared by stirring the mixture of AuNPs and OMC at room temperature. Generally, the ratio of AuNPs and OMC might greatly affect the morphology and the electrochemical conductivity of the nanocomposite. Although a low-concentration of AuNPs could decrease the

conductivity of the nanocomposite, a high-concentration of AuNPs might result in the aggregation or fusion of AuNPs, which will in turn lead to a decline in the electron conductivity of the nanocomposite and lower the antibody loading. As a result, the comparative study was carried out by synthesizing a series of OMC-AuNPs nanocomposites with different ratios of AuNPs to OMC from 1:5 to 4:5.

Since the detectable signal was derived from the thionine (Th) assembled on the OMC-AuNPs in the immunosensor, CV measurements were performed in PBS after Th was further assembled with OMC-AuNPs, and the evaluation was based on the peak current intensity of Th in the assembly. As a control, Th was assembled on the surface of GCE directly by a covalent linking between the amino group on Th and the carboxyl group on GCE, which was produced via an electrochemical oxidation of GCE in 0.5 M H_2SO_4.[30] As shown in Figure 1a, both Th/GCE and Th/OMC-AuNPs/GCE displayed a pair of redox peaks, while the OMC-AuNPs/GCE did not show any redox wave, suggesting that the redox peaks could be ascribed to the redox waves of Th on the electrode, and the redox property of Th was retained after the assembly. It should be noted that the peak current for the Th/OMC-AuNPs/GCE was much higher than that for Th/GCE, indicating that OMC-AuNPs nanocomposite played an important role in both enhancing the surface area and improving the electron transfer of Th on the electrode. As shown in Figure 1b, increasing the ratio of AuNPs: OMC from 1:5 to 2:5 resulted in an increase of the peak current, while further increasing the ratio made the peak current gradually decreased. Therefore, the Th/OMC-AuNPs displayed the best electrochemical performance at a AuNPs: OMC ratio of 2:5.

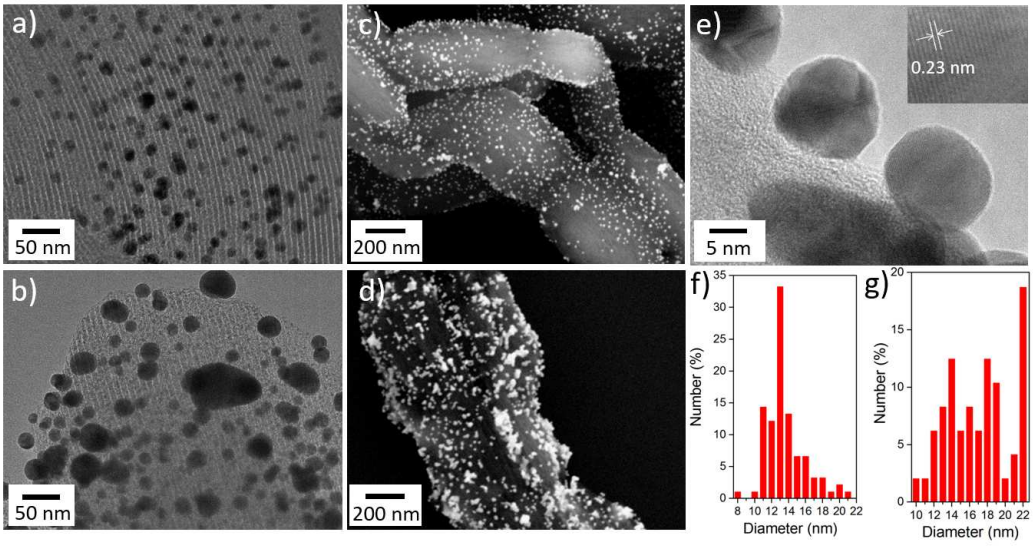

Figure 2. TEM (a, b) and SEM (c, d) images of OMC-AuNPs nanocomposite with a AuNPs: OMC ratio of 2:5 (a, c) and 4:5 (b, d); TEM image of AuNPs in the OMC-AuNPs nanocomposite with a AuNPs: OMC ratio of 2:5 (e), and histogram of the AuNPs particles size summarized according to the TEM images in a) and b), respectively (f, g). The inset in e) is the high resolution image of AuNPs in the OMC-AuNPs nanocomposite with a AuNPs: OMC ratio of 2:5.

To further get insight in the reason for effect of AuNPs/OMC ratio on the electrochemical performance of the nanocomposite, the morphology of the OMC-AuNPs with different AuNPs/OMC ratios were investigated. Figure 2 presented the TEM and SEM images of OMC-AuNPs nanocomposite with AuNPs: OMC ratios of 2:5 and 4:5, respectively. When the ratio was 2:5, AuNPs were uniformly decorated on OMC (Figure 2a, 2c, 2e and 2f), with a size around at 13 nm. The lattice fringes shown in the inset of Figure 2e were visible with a spacing of about 0.23 nm, which was corresponding to the lattice spacing of the (111) planes of Au, indicating that AuNPs on the surface of OMC remained the original structure. However, when the ratio increased to 4:5, the diameter of AuNPs became much larger and became aggregated or fused (Figure 2b and 2d), and the size distribution of AuNPs was not uniform any more (Figure 2g). Thus, the poor electrochemical performance of the Th/OMC-AuNPs/GCE with a AuNPs: OMC ratio of 4:5 could be ascribed to the

aggregation of AuNPs on the surface of OMC.

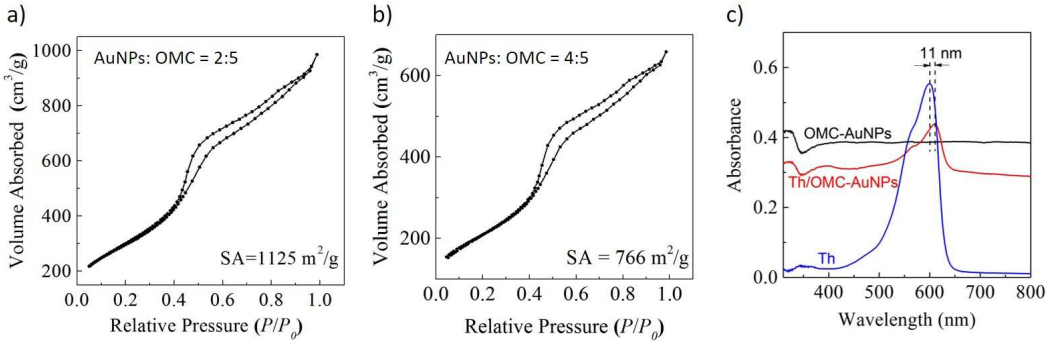

Figure 3. Nitrogen adsorption-desorption isotherms of OMC-AuNPs nanocomposites with AuNPs: OMC ratio of 2:5 (a) and 4:5 (b), respectively, and UV-vis absorption spectra of Th, Th/OMC-AuNPs and OMC-AuNPs (c).

The surface area of OMC-AuNPs nanocomposites with different AuNPs: OMC ratios were evaluated by Brunauer–Emmett–Teller (BET) analysis of nitrogen adsorption-desorption isotherms (Figure 3a and 3b). It was found that the surface area of OMC-AuNPs nanocomposite with a ratio of 2:5 was about 1125 $m^2 \bullet g^{-1}$, while the surface area for that with a ratio of 4:5 was about 766 $m^2 \bullet g^{-1}$. On one hand, the increased ratio of AuNPs: OMC led to an aggregation or fusion of AuNPs, thus resulting in a decreased surface area of the AuNPs. On the other hand, with increasing AuNPs concentration in the nanocomposite, the amount of the mesoporous OMC accordingly decreased, which made the total surface area reduced. Therefore, OMC-AuNPs nanocomposite with a ratio of 2:5 can provide more surface active sites and make electron transfer easier, which was consistent with the CV results and morphology observation. Herein, the AuNPs: OMC ratio of 2:5 was selected for the nanocomposite preparation in the following study.

The assembly of OMC-AuNPs and Th in solution was further characterized by UV-vis spectra. As shown in Figure 3c, both the Th and Th/OMC-AuNPs displayed two characteristic adsorption peaks at ca. 568 nm and 600 nm, which can be ascribed to the monomeric Th and the T-type dimer aggregate, respectively, indicating that the intrinsic properties of Th were preserved after the assembly with OMC-AuNPs.[36,37] It should be noted that the obvious baseline difference between the spectra of Th and

those of OMC-AuNPs and Th/OMC-AuNPs could be ascribed to the scattering effect of OMC. Interestingly, a red shift up to 11 nm of the n−π* transition of the C=N bond for Th (from 600 nm to 611 nm) was observed after the assembly with OMC-AuNPs, implying an electron transfer between OMC-AuNPs and Th, which would be highly desirable for the electrochemical detection in the proposed immunosensor.

Thermal stability of Nb

Since thermal stability of Nb is critical for its real applications, the activity of Nb was evaluated by ELISA after incubating at 37°C and 70°C for 0.5, 1 and 2 h, respectively. As a control, the thermal stability of conventional monoclonal antibody for CP4-EPSPS (mAb) was also detected with a similar way. As shown in Figure 4, after being treated at 37°C, the Nb and mAb kept similar activity. However, the Nb remained much higher activity than mAb after the treatment at 70°C, especially in an elongated time. For instance, after be incubating at 70°C for 2 h, Nb still remained for approximately 60% activity, while mAb lost almost all activity. Hence, the high thermal stability of Nb will make it possible to be applied in more applications, especially those requires high temperature, and are typically prohibited by the low thermal stability of conventional antibodies.

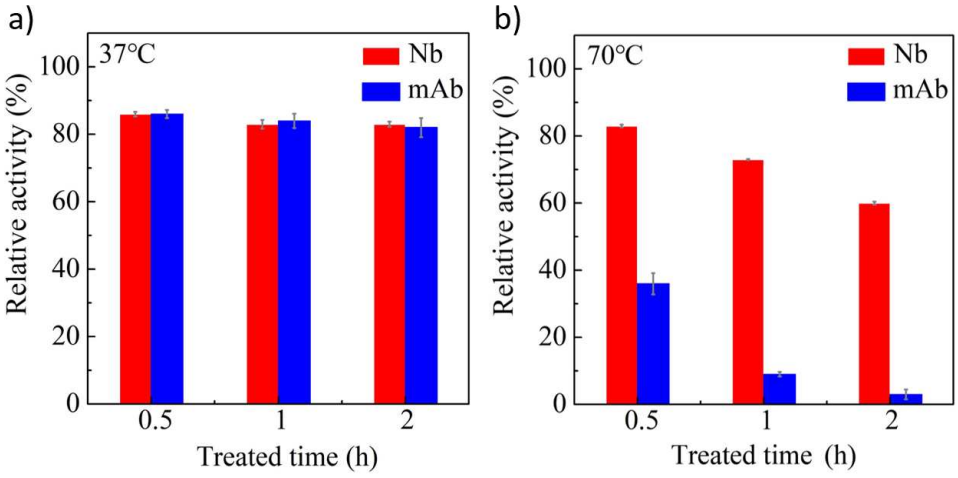

Figure 4. Activity of Nb and mAb after incubating at 37 °C (a) and 70 °C (b) for 0.5 h, 1 h and 2 h.

Fabrication of the Electrochemical Immunosensor

The fabrication process of the electrochemical immunosensor was monitored by cyclic voltammetry (CV) measurements in 0.1 M PBS solution containing 2 mM $K_3[Fe(CN)_6]$. As shown in Figure 5a, the CV of bare GCE showed a pair of clear redox peaks with the anodic and cathodic peak potential difference of less than 85 mV, demonstrating a reversible redox reaction process. After the modification of the OMC-AuNPs onto GCE, the current intensity became more remarkable than that of bare GCE, which could be ascribed to the enhanced electron transfer activity of OMC-AuNPs. The redox peak currents decreased progressively after Th-Nb and BSA were successively assembled on the surface of GCE, suggesting that the electron transfer of $K_3[Fe(CN)_6]$ at the electrode surface was blocked by the proteins. With the further incubation with CP4-EPSPS, the resistance of the CP4-EPSPS further inhibited the electron transfer of $K_3[Fe(CN)_6]$ at the electrode surface and decreased current was obtained. All the above results confirmed that the electrochemical immunosensor was successfully fabricated.

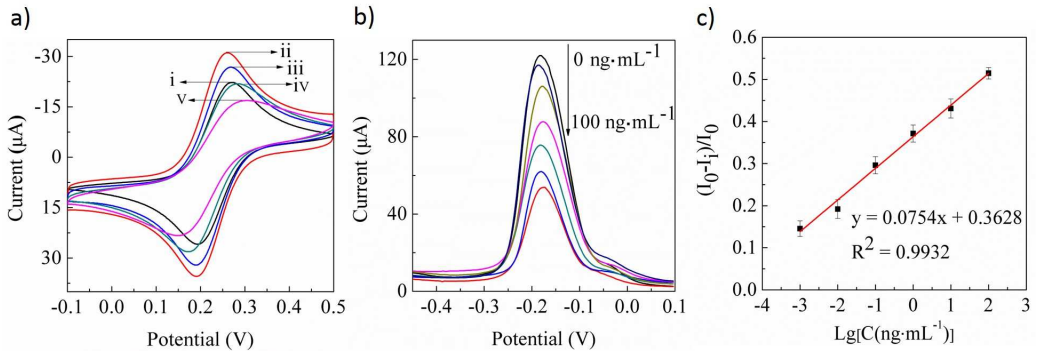

Figure 5. (a) CV curves of modified GCE in 0.1 M PBS solution containing 2 mM $K_3[Fe(CN)_6]$ during each step of the immunosensor fabrication: (i) bare GCE, (ii) OMC-AuNPs/GCE, (iii) Th-Nb/OMC-AuNPs/GCE, (iv) BSA/Th-Nb/OMC-AuNPs/GCE, (v) CP4-EPSPS/BSA /Th-Nb/OMC-AuNPs/GCE. (b) DPV curves of the immunosensor with different concentrations of CP4-EPSPS in N_2-saturated PBS (0.1 M, pH 7.4). (c) Calibration curve for the CP4-EPSPS immunosensor.

Given the excellent redox behavior of Th/OMC-AuNPs as shown in Figure 1, the modified Th probe was applied for the detection of CP4-EPSPS quantitatively and sensitively by DPV technique. As shown in Figure 5b, without the addition of CP4-EPSPS, an oxidation peak appeared at around -0.17 V in the DPV curve, which was consistent with the results in Figure 1 and thus the oxidation peak could be ascribed to the electrochemical oxidation of Th on the electrode. After the addition of CP4-EPSPS and further increasing the concentration, the DPV peak currents decreased gradually. The electrochemical oxidation/reduction process of Th involves not only the electron transfer between Th and electrode, but also the charge transfer at the electrolyte/electrode interface. Therefore, for the immunosensor in our work, the electrochemical signal of Th not only depends on the amount of Th immobilized on the electrode, but also relies on the resistance of the membrane on the electrode. Upon the formation of immunocomplex, the membrane resistance increased, thus the electrochemical oxidation/reduction current decreased accordingly. In light of the electrochemical current reduction in the immunoreaction process, it could be deduced that an electrochemical immunosensor can be developed for the detection of CP4-EPSPS.[38,39] Figure 5c showed a calibration curve with a good linear relationship between the current decrease ratios $(I_0-I_i)/I_0$ and logarithm values of CP4-EPSPS concentrations in the range from 0.001 to 100 ng•mL^{-1}, where I_0 and I_i represented the currents before and after the capture of different concentrations of CP4-EPSPS. The regression equation could be denoted as $(I_0-I_i)/I_0 = 0.0754\text{LogC}$ (ng•mL^{-1}) + 0.3628 with a correlation coefficient of 0.9932. The limit of detection (LOD) was 0.72 pg•mL^{-1} based on the equation of LOD = 3σ/S (σ is the standard deviation of blank samples data and S is the slope of calibration curve), which was more than 3 orders of magnitude lower than those of previously reported works (Table 1).[13, 40,41] Moreover, the LOD was also much lower than that of the commercial test kit of CP4-EPSPS (such as Quantiplate Kit CP4-EPSPS in corn & soy, USA, LOD = 1 mg•mL^{-1}).[42] Hence, the prepared immunosensor could be used for the detection of CP4-EPSPS quantitatively and efficiently accordingly. The high sensitivity of the as-obtained

immunosensor could be ascribed to the synergetic coupling of Nb and carbon nanomaterials. On one hand, compared with conventional mAb, Nb had a more comparable size (15 kDa) with that of CP4-EPSPS (~40 kDa). As a result, the capture of CP4-EPSPS by Nb would lead to a more obvious signal change, i.e., higher sensitivity, than that using conventional mAb. On the other hand, the OMC-AuNPs with high surface area and electron mobility could offer sufficient electron conductivity and active anchoring sites for assembling Nbs and the redox probe, which was favor of improving the sensor sensitivity. Therefore, the immunosensor presented here displayed much lower detection limit compared with those of other previously reported studies, offering an alternative way for the determination of the CP4-EPSPS level in food and agroproducts.

Table 1. Comparison of a few available methods for CP4-EPSPS detection.

Method	Capture agent	Linear range ($ng \cdot mL^{-1}$)	LOD ($pg \cdot mL^{-1}$)	References
Electrochemical immunosensor	Nb	0.001–100	0.72	This work
SPR	DNA	$50–5\times10^{3}$	5×10^{4}	13
LC-MS/MS	specific peptides	$250–5\times10^{4}$	1×10^{5}	38
Fluorescent immunosensor	Nb	5–100	340	39
Commercial test kit	—	—	1×10^{6}	40

Specificity, stability, reproducibility and reliability of the immunosensor

To investigate the specificity of the immunoassay, the immunosensor was incubated with Cry1Aa, Cry1B, and Cry1F as interfering proteins. As shown in Figure 6a, the current decrease ratios $(I_0-I_i)/I_0$ of Cry1Aa, Cry1B, and Cry1F were much lower than that of CP4-EPSPS, indicating that the immunosensor presented high selectivity and

specificity for CP4-EPSPS. The high specificity of the as-constructed immunosensor further proved our speculation that the immunoreaction between CP4-EPSPS and Nb immobilized on the electrode was the main reason for the reduction of electrochemical current of Th. To investigate the stability of the immunosensor, the prepared immunosensors were stored in 0.1 M PBS (pH = 7.4) at 4°C. As shown in Figure 6b, the constructed immunosensors still kept 94%, 87.3% and 83.2% of initial response for 10 ng•mL^{-1} CP4-EPSPS after the storage in 0.1 M PBS of pH 7.4 at 4°C for 1 day, 6 days and 14 days, respectively, which suggested that the constructed immunosensor had a satisfactory stability. Furthermore, the reproducibility of the immunosensor was evaluated by determining five immunosensors, respectively. The variation coefficient was 4.2 % (n=5) at 10 ng•mL^{-1} CP4-EPSPS solution, demonstrating a good reproducibility of the immunosensor.

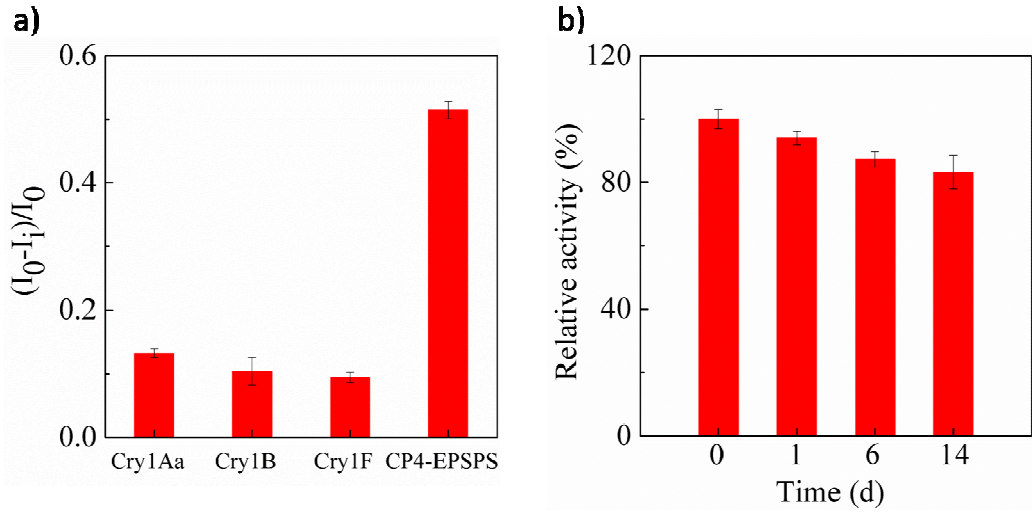

Figure 6. (a) The decrease ratio of DPV peak current of the immunosensor for Cry1Aa, Cry1B, Cry1F, and CP4-EPSPS with a concentration of 100 ng•mL^{-1} in PBS solution. (b) The stability of the immunosensor for CP4-EPSPS (10 ng•mL^{-1}) detection after 1 day, 6 days, and 14 days.

Table 2. Recovery tests of CP4-EPSPS from spiked nontransgenic soybean extract samples.

Entry	Spiked CP4-EPSPS ($ng•mL^{-1}$)	Found ($ng•mL^{-1}$)	Recovery (%)	RSD (%) (n= 3)
1	1	0.97	97	2.7
2	10	10.27	102.7	3.6
3	100	96.18	96.18	3.3

To further validate the reliability of this immunosensor, the recovery experiment was performed by analyzing the CP4-EPSPS protein-spiked nontransgenic soybean extract samples with three concentrations (1, 10, 100 $ng•mL^{-1}$). As shown in Table 2, the results displayed acceptable recoveries of the spiked samples between 96.18% and 102.7% with a relative standard deviation (RSD) less than 3.6%, indicating a good accuracy of the electrochemical immunoassay for quantitative detection of CP4-EPSPS based on the OMC-AuNPs nanocomposite and Nb.

Conclusions

In summary, a simple electrochemical immunoassay with high sensitivity and efficiency was developed for the detection of CP4-EPSPS by coupling Nb, OMC and Th. OMC not only had excellent conductivity and large surface area, but also provided abundant binding sites by cooperating with AuNPs for the conjugation of Nb and Th that were acted as capture agent and electrochemical probe, respectively. As a result, the as-constructed immunosensor exhibited a wide linear range, high stability and satisfactory reproducibility for CP4-EPSPS detection, and more strikingly, its sensitivity was at least 3 orders of magnitude higher than those by other methods and the commercial CP4-EPSPS kit. The convenient operation and ultrahigh sensitivity of the proposed immunoassay method would open a new vista in the field of food safety detection.

Acknowledgements

This work is supported by the National Natural Science Foundation of China (21675022, 21775018 and 81773624), Program from the Natural Science Foundation of Jiangsu Province (BK20170084 and BK20160028), Social Development Project of Jiangsu Province (BE2017746), and the Fundamental Research Funds for the Central Universities.

References

(1) Schaart, J. G.; van de Wiel, C. C. M.; Lotz, L. A. P.; Smulders, M. J. M. Opportunities for Products of New Plant Breeding Techniques. *Trends Plant Sci* **2016**, *21*, 438-449.

(2) Azadi, H.; Samiee, A.; Mahmoudi, H.; Jouzi, Z.; Khachak, P. R.; De Maeyer, P.; Witlox, F. Genetically modified crops and small-scale farmers: main opportunities and challenges. *Crit. Rev. Biotechnol.* **2016**, *36*, 434-446.

(3) Moshelion, M.; Altman, A. Current challenges and future perspectives of plant and agricultural biotechnology. *Trends Biotechnol.* **2015**, *33*, 337-342.

(4) Mickelbart, M. V.; Hasegawa, P. M.; Bailey-Serres, J. Genetic mechanisms of abiotic stress tolerance that translate to crop yield stability. *Nat. Rev. Genet.* **2015**, *16*, 237-251.

(5) Tsatsakis, A. M.; Nawaz, M. A.; Tutelyan, V. A.; Golokhvast, K. S.; Kalantzi, O.-I.; Chung, D. H.; Kang, S. J.; Coleman, M. D.; Tyshko, N.; Yang, S. H.; Chung, G. Impact on environment, ecosystem, diversity and health from culturing and using GMOs as feed and food. *Food Chem. Toxicol.* **2017**, *107*, 108-121.

(6) Marani, M. M.; Costa, J.; Mafra, I.; Oliveira, M.; Camperi, S. A.; Leite, J. In Silico Peptide Prediction for Antibody Generation to Recognize 5-Enolpyruvylshikimate-3-Phosphate Synthase (EPSPS) in Genetically Modified Organisms. *Biopolymers.* **2015**, *104*, 91-100.

(7) Herrera-Agudelo, M. A.; Miro, M.; Arruda, M. A. Z. In vitro oral

bioaccessibility and total content of Cu, Fe, Mn and Zn from transgenic (through cp4 EPSPS gene) and nontransgenic precursor/successor soybean seeds. *Food Chem.* **2017**, *225*, 125-131.

(8) Guo, J.; Chen, L.; Liu, X.; Gao, Y.; Zhang, D.; Yang, L. A multiplex degenerate PCR analytical approach targeting to eight genes for screening GMOs. *Food Chem.* **2012**, *132*, 1566-1573.

(9) Zhang, M.; Gao, X.; Yu, Y.; Ao, J.; Qin, J.; Yao, Y.; Li, Q. Detection of Roundup Ready soy in highly processed products by triplex nested PCR. *Food Control* **2007**, *18*, 1277-1281.

(10) Huber, I.; Block, A.; Sebah, D.; Debode, F.; Morisset, D.; Grohmann, L.; Berben, G.; Stebih, D.; Milavec, M.; Zel, J.; Busch, U. Development and Validation of Duplex, Triplex, and Pentaplex Real-Time PCR Screening Assays for the Detection of Genetically Modified Organisms in Food and Feed. *J. Agr. Food Chem.* **2013**, *61*, 10293-10301.

(11) Wang, C.; Li, R.; Quan, S.; Shen, P.; Zhang, D.; Shi, J.; Yang, L. GMO detection in food and feed through screening by visual loop-mediated isothermal amplification assays. *Anal. Bioanal. Chem.* **2015**, *407*, 4829-4834.

(12) Ocana, M. F.; Fraser, P. D.; Patel, R. K. P.; Halket, J. M.; Bramley, P. M. Evaluation of stable isotope labelling strategies for the quantitation of CP4 EPSPS in genetically modified soya. *Anal. Chim. Acta* **2009**, *634*, 75-82.

(13) Jang, H.; Kwak, C. H.; Kim, G.; Kim, S. M.; Huh, Y. S.; Jeon, T. J. Identification of genetically modified DNA found in Roundup Ready soybean using gold nanoparticles. *Microchim Acta* **2016**, *183*, 2649-2654.

(14) Bookout, J. T.; Joaquim, T. R.; Magin, K. M.; Rogan, G. J.; Lirette, R. P. Development of a dual-label time-resolved fluorometric immunoassay for the simultaneous detection of two recombinant proteins in potato. *J. Agr. Food Chem.* **2000**, *48*, 5868-5873.

(15) Rogan, G. J.; Dudin, Y. A.; Lee, T. C.; Magin, K. M.; Astwood, J. D.; Bhakta, N. S.; Leach, J. N.; Sanders, P. R.; Fuchs, R. L. Immunodiagnostic methods for detection of 5-enolpyruvylshikimate-3-phosphate synthase in Roundup

Ready (R) soybeans. *Food Control* **1999**, *10*, 407-414.

(16) Shen, W.-J.; Zhuo, Y.; Chai, Y.-Q.; Yang, Z.-H.; Han, J.; Yuan, R. Enzyme-Free Electrochemical Immunosensor Based on Host-Guest Nanonets Catalyzing Amplification for Procalcitonin Detection. *ACS Appl. Mater. Interfaces* **2015**, *7*, 4127-4134.

(17) Liu, T.-Z.; Hu, R.; Zhang, X.; Zhang, K.-L.; Liu, Y.; Zhang, X.-B.; Bai, R.-Y.; Li, D.; Yang, Y.-H. Metal-Organic Framework Nanomaterials as Novel Signal Probes for Electron Transfer Mediated Ultrasensitive Electrochemical Immunoassay. *Anal. Chem.* **2016**, *88*, 12516-12523.

(18) Zhai, Q.; Zhang, X.; Li, J.; Wang, E. Molybdenum carbide nanotubes: a novel multifunctional material for label-free electrochemical immunosensing. *Nanoscale* **2016**, *8*, 15303-15308.

(19) Liang, Y.-R.; Zhang, Z.-M.; Liu, Z.-J.; Wang, K.; Wu, X.-Y.; Zeng, K.; Meng, H.; Zhang, Z. A highly sensitive signal-amplified gold nanoparticle-based electrochemical immunosensor for dibutyl phthalate detection. *Biosens. Bioelectron.* **2017**, *91*, 199-202.

(20) Zhou, Y.; Marar, A.; Kner, P.; Ramasamy, R. P. Charge-Directed Immobilization of Bacteriophage on Nanostructured Electrode for Whole-Cell Electrochemical Biosensors. *Anal. Chem.* **2017**, *89*, 5735-5742.

(21) Ren, K.; Wu, J.; Ju, H.; Yan, F. Target-Driven Triple-Binder Assembly of MNAzyme for Amplified Electrochemical Immunosensing of Protein Biomarker. *Anal Chem* **2015**, *87*, 1694-1700.

(22) Lee, J. S.; Joo, S. H.; Ryoo, R. Synthesis of mesoporous silicas of controlled pore wall thickness and their replication to ordered nanoporous carbons with various pore diameters. *J. Am. Chem. Soc.* **2002**, *124*, 1156-1157.

(23) Zhi, J.; Zhao, W.; Liu, X.; Chen, A.; Liu, Z.; Huang, F. Highly Conductive Ordered Mesoporous Carbon Based Electrodes Decorated by 3D Graphene and 1D Silver Nanowire for Flexible Supercapacitor. *Adv. Funct. Mater.* **2014**, *24*, 2013-2019.

(24) Yang, Y.; Cao, Y.; Wang, X.; Fang, G.; Wang, S. Prussian blue mediated

amplification combined with signal enhancement of ordered mesoporous carbon for ultrasensitive and specific quantification of metolcarb by a three-dimensional molecularly imprinted electrochemical sensor. *Biosens. Bioelectron.* **2015**, *64*, 247-254.

(25) Li, Y.; Zhai, X.; Liu, X.; Wang, L.; Liu, H.; Wang, H. Electrochemical determination of bisphenol A at ordered mesoporous carbon modified nano-carbon ionic liquid paste electrode. *Talanta* **2016**, *148*, 362-369.

(26) Regiart, M.; Fernandez-Baldo, M. A.; Villarroel-Rocha, J.; Messina, G. A.; Bertolino, F. A.; Sapag, K.; Timperman, A. T.; Raba, J. Microfluidic immunosensor based on mesoporous silica platform and CMK-3/poly-acrylamide-co-methacrylate of dihydrolipoic acid modified gold electrode for cancer biomarker detection. *Anal. Chim. Acta* **2017**, *963*, 83-92.

(27) Qiang, Z.; Chen, Y.-M.; Gurkan, B.; Guo, Y.; Cakmak, M.; Cavicchi, K. A.; Zhu, Y.; Vogt, B. D. Cooperatively assembled, nitrogen-doped, ordered mesoporous carbon/iron oxide nanocomposites for low-cost, long cycle life sodium-ion batteries. *Carbon* **2017**, *116*, 286-293.

(28) Cabanas-Danes, J.; Rodrigues, E. D.; Landman, E.; Van Weerd, J.; van Blitterswijk, C.; Verrips, T.; Huskens, J.; Karperien, M.; Jonkheijm, P. A Supramolecular Host-Guest Carrier System for Growth Factors Employing VHH Fragments. *J. Am. Chem. Soc.* **2014**, *136*, 12675-12681.

(29) De Meyer, T.; Muyldermans, S.; Depicker, A. Nanobody-based products as research and diagnostic tools. *Trends Biotechnol* **2014**, *32*, 263-270.

(30) Li, G.; Zhu, M.; Ma, L.; Yan, J.; Lu, X.; Shen, Y.; Wan, Y. Generation of Small Single Domain Nanobody Binders for Sensitive Detection of Testosterone by Electrochemical Impedance Spectroscopy. *ACS Appl. Mater. Interfaces* **2016**, *8*, 13830-13839.

(31) Wang, H.; Li, G.; Zhang, Y.; Zhu, M.; Ma, H.; Du, B.; Wei, Q.; Wan, Y. Nanobody-Based Electrochemical Immunoassay for Ultrasensitive Determination of Apolipoprotein-A1 Using Silver Nanoparticles Loaded Nanohydroxyapatite as Label. *Anal Chem* **2015**, *87*, 11209-11214.

(32) Zhou, Q.; Li, G.; Zhang, Y.; Zhu, M.; Wan, Y.; Shen, Y. Highly Selective and Sensitive Electrochemical Immunoassay of Cry1C Using Nanobody and pi-pi Stacked Graphene Oxide/Thionine Assembly. *Anal. Chem.* **2016**, *88*, 9830-9836.

(33) Daniel, M. C.; Astruc, D. Gold nanoparticles: Assembly, supramolecular chemistry, quantum-size-related properties, and applications toward biology, catalysis, and nanotechnology. *Chem. Rev.* **2004**, *104*, 293-346.

(34) Wu, D.; Guo, A.; Guo, Z.; Xie, L.; Wei, Q.; Du, B. Simultaneous electrochemical detection of cervical cancer markers using reduced graphene oxide-tetraethylene pentamine as electrode materials and distinguishable redox probes as labels. *Biosens. Bioelectron.* **2014**, *54*, 634-639.

(35) Fang, G.; Liu, G.; Yang, Y.; Wang, S. Quartz crystal microbalance sensor based on molecularly imprinted polymer membrane and three-dimensional Au nanoparticles@mesoporous carbon CMK-3 functional composite for ultrasensitive and specific determination of citrinin. *Sensors Actuators B: Chem* **2016**, *230*, 272-280.

(36) Das, S.; Kamat, P. V. Can H-aggregates serve as eight-harvesting antennae? Triplet-triplet energy transfer between excited aggregates and monomer thionine in aersol-OT solutions. *J Phys Chem B* **1999**, *103*, 209-215.

(37) Li, Q. W.; Zhang, J.; Yan, H.; He, M. S.; Liu, Z. F. Thionine-mediated chemistry of carbon nanotubes. *Carbon* **2004**, *42*, 287-291.

(38) Yu, X. Y.; Wang, Y. Y.; Chen, X. M.; Wu, K. B.; Chen, D. C.; Ma, M.; Huang, Z. J.; Wu, W. Z.; Li, C. Y. White-Light-Exciting, Layer-by-Layer-Assembled ZnCdHgSe Quantum Dots/Polymerized Ionic Liquid Hybrid Film for Highly Sensitive Photoelectrochemical lmmunosensing of Neuron Specific Enolase. *Anal. Chem.* **2015**, *87*, 4237-4244.

(39) Zhu, X. Q.; Zhai, Q. F.; Gu, W. L.; Li, J.; Wang, E. K. High-Sensitivity Electrochemiluminescence Probe with Molybdenum Carbides as Nanocarriers for alpha-Fetoprotein Sensing. *Anal. Chem.* **2017**, *89*, 12108-12114.

(40) Yin, K.; Liu, A.; Li, S.; Mi, L.; Liu, X.; Liu, Y.; Zhao, Y.; Li, Y.; Wei, W.;

Zhang, Y.; Liu, S. Construction of iron-polymer-graphene nanocomposites with low nonspecific adsorption and strong quenching ability for competitive immunofluorescent detection of biomarkers in GM crops. *Biosens. Bioelectron.* **2017**, *90*, 321-328.

(41) Zhang, M.; Teng, Z.; Xu, W.; Dai, R.; Qing, H.; Deng, Y.; Xu, J. Quantification of CP4 EPSPS in genetically modified Nicotiana tabacum leaves by LC-MS/MS with 18O-labelling. *Anal. Methods* **2014**, *6*, 7399-7406.

(42) https://www.envirologix.com/catalog/188-10448-qualiplate-kit-for-detection-of-cp4-epsps-1-platekit/.

For TOC Only